Processable Star-Shaped Molecules with Triphenylamine Core as Hole-Transporting Materials: Experimental and Theoretical Approach

Noura Metri, Xavier Sallenave, Cedric Plesse, Layla Beouch, Pierre-Henri Aubert, Fabrice Goubard, Claude Chevrot, Gjergji Sini

Processable Star-Shaped Molecules with Triphenylamine Core as Hole-Transporting Materials: Experimental and Theoretical Approach

Noura Metri, Xavier Sallenave, Cédric Plesse, Layla Beouch, Pierre-Henri Aubert, Fabrice Goubard, Claude Chevrot, and Gjergji Sini*

Laboratoire de Physicochimie des Polymères et des Interfaces, Université de Cergy-Pontoise, 5 mail Gay Lussac, 95031 Cergy-Pontoise Cedex, France

ABSTRACT: In this study we report on the characterization of five star-shaped π-conjugated molecules by means of UV− vis absorption spectroscopy and electrochemical cyclic voltammetry. These molecules, with triphenylamine (TPA) core bearing one thienothiophene moiety and a different number of thiophene ones, are designed as hole-transporting materials for dye-sensitized solar cell (DSSC) applications. Theoretical calculations employing the B3LYP functional are also carried out in order to understand the structure−property relationships. UV−vis absorption measurements and time-dependent density functional theory (TDDFT) calculations show the presence of intense UV−vis bands for all compounds. These bands are dominated by two degenerate π−π* excitations mostly involving the HOMO → LUMO and HOMO → LUMO+1 transitions. Electrochemical cyclic voltammetry and DFT calculations show the HOMO (LUMO) energy levels increasing (decreasing) with the number of conjugated heterocyclic rings in these molecules. The HOMO energies have been found to vary between −5.38 and −5.13 eV thus showing good positioning with respect to the Fermi level of gold electrode (DSSC applications). The calculated internal reorganization energies (λi) suggest for these materials promising hole-transport properties. The analysis of the space extension of the HOMO orbitals as a function of the number of conjugated rings in these molecules gives useful information on their design.

1. INTRODUCTION

Solar cells are one of the most promising alternatives for energy conversion. Among various strategies, dye-sensitized solar cells (DSSCs)[1] have attracted a lot of attention, and a large amount of research and development has been dedicated to this field over the past two decades. In a DSSC device, light is absorbed by the dye anchored on the TiO_2 surface, and then electrons from the excited dye are injected into the conduction band of the TiO_2, which generates an electric current. The ground state of the dye is regenerated by the electrolyte which contains a redox couple I_3^-/I^- mediator to give efficient charge separation. For a decade, a promising type of DSSC has been developed: contrary to the electrolyte cell, it is based on a heterojunction between the dye-sensitized TiO_2 and an organic hole-conducting material. Recently an overall efficiency of 6% was achieved.[2]

While dye properties are very important for these devices, we focus here on the role of the hole-transporting materials. A variety of organic hole-transporting materials have been described, and efficiencies higher than 5% have been obtained by using compounds such as amorphous 2,2′,7,7′-tetrakis-(*N*,*N*-di-*p*-methoxyphenylamine)9,9′-spirobifluorene (spiro-OMeTAD) as a hole-transporting material.[3,4]

Among the various classes of organic hole-transporting materials,[5] special attention has been paid to compounds derived from triphenylamine (TPA).[6−8] These compounds (possessing three-dimensional geometry) can lead to amorphous materials with interesting optical and charge-transport properties as shown by many research groups who have designed such materials for a variety of photovoltaic devices.[9−13]

Different π-conjugated ring molecules can be used to extend the π-conjugated system of the TPA core. Star-shaped molecules containing TPA core and thiophene (Th) derivatives have yielded interesting results in DSSC applications.[14−16] Another promising candidate, which can be combined with these star-shaped molecules, is the thieno[3,2-*b*]thiophene (TTh) group which contains two fused thiophene rings. Actually, compared to its analogue, Th−Th, the TTh compound offers better π-conjugation and smaller geometric relaxation energy upon oxidation.

Based on these observations, we recently reported the synthesis of five star-shaped molecules containing various combinations of Th and thieno[3,2-*b*]thiophene−C_9H_{19} (TTh−C_9) located in the arms linked to the TPA core (Chart 1).[17] Preliminary results concerning the optical properties of these molecules have shown promising properties for use in photovoltaic applications.

Chart 1. Triphenylamine (TPA) Derivatives (1−5) Bearing Different π-Conjugated Arms

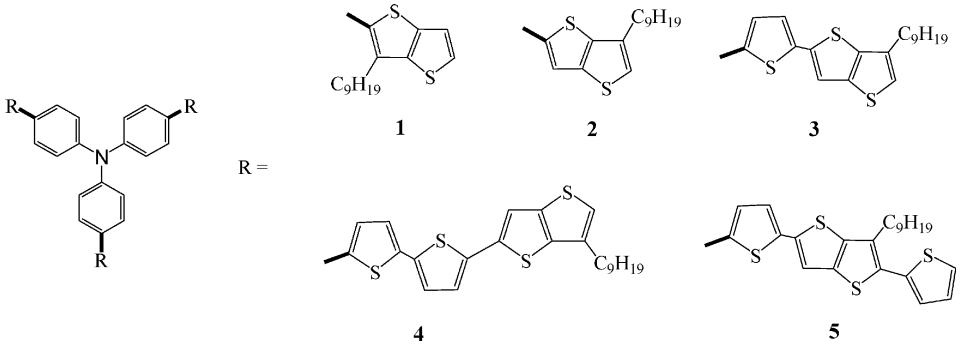

From a theoretical point of view, the hole-transport properties in these materials are mainly discussed in terms of disorder models.[18] While mobility calculations based on first-principles are still a challenge,[19,20] determination of charge-transfer rate constants (k_{HT}) based on the Marcus theory can provide very useful information.[21−24] Limiting the discussion to the case of amorphous materials, the elementary step of the charge transport can be seen as a charge transfer (CT) between two adjacent molecules. In such a case, the rate constant of a hole-transfer reaction can be described by the "hopping" mechanism and calculated using the following equation:[21−24]

$$k_{HT} = \frac{4\pi^2}{h}\frac{1}{\sqrt{4\pi\lambda k_B T}} t^2 \exp\left[\frac{-(\Delta G^\circ + \lambda)^2}{4k_B\lambda T}\right] \quad (1)$$

In this equation, t is the electronic coupling between two adjacent molecules, ΔG° is the free energy of the hole-transfer reaction (which is zero in the case of hole transfer between identical molecules), and λ is the reorganization energy. This parameter is the sum of two terms: (i) λ_s, containing the contribution from the medium polarization energy, and (ii) λ_i, representing the energetic effort due to the intramolecular geometric relaxations related to the hole transfer between two adjacent molecules.

Knowledge of the three parameters is necessary in order to determine the k_{HT} constant between two adjacent molecules, and still additional parameters need to be known in order to evaluate hole mobility. However, in a series of similar compounds, each of these parameters considered individually can provide trends which could be helpful in the design of new materials. In the case of a family of similar amine compounds for instance, a good correlation between the trends of the λ values and the experimental hole mobilities has been observed.[25]

Other molecular electronic parameters such as the HOMO and LUMO level energies and their space distributions within the molecular backbone are extensively used in order to evaluate the optical properties of these materials and the efficiency of the film−electrode (film−dye) contact properties but also to predict their charge-transport properties.[26−29]

In the present work, we report a detailed investigation of some of these properties by comparing experimental and theoretical results. UV−vis measurements and electrochemical cyclic voltammetry were performed in order to assess various parameters (HOMO and LUMO level energies and their band gap, spectral absorption domains, and extinction coefficients). Calculations based on various density functional theory (DFT)[30] methods (especially B3LYP[31,32]) were also carried out in order to understand the impact of the structural and electronic properties of these molecules on their optical properties, geometrical relaxation energies (λ_i), and their potential use as hole-transporting materials in solar cell applications.

2. EXPERIMENTAL SECTION

2.1. Materials. All chemicals were purchased from Aldrich or Fischer Scientific without further purification. All solvents, unless otherwise stated, were of analytical grade, purist quality and used as received from VWR international. Tris(4-(3-nonylthieno[3,2-*b*]thiophen-2-yl)phenyl)amine **1**, tris(4-(3-nonylthieno[3,2-*b*]thiophen-5-yl)phenyl)amine **2**, tris(4-(5-(3-nonylthieno[3,2-*b*]thiophen-5-yl)thiophen-2-yl)phenyl)amine **3**, tris(4-(5-(5-(3-nonylthieno[3,2-b]thiophen-5-yl)thiophen-2-yl)thiophen-2-yl)phenyl)amine **4**, and tris(4-(5-(3-nonyl-2-(thiophen-2-yl)thieno[3,2-b]thiophen-5-yl)thiophen-2-yl)-phenyl)amine **5** were synthesized according to the procedure described in the literature.[17] The structures of these molecules are shown in Chart 1.

2.2. Instruments and Measurements. UV−vis absorption spectra were taken with a Jasco (V-570) UV−vis−NIR spectrophotometer. The cyclic voltammetry was carried out in a glovebox using a Princeton Applied Research-Potentiostat/Galvanostat model 273A (EG&G, The Netherlands). The electrochemical setup was a three-electrode single cell, with a glassy carbon (GC) disk (2 mm diameter) coated with the sample film as the working electrode, a Pt wire as counter electrode, and a silver wire pseudoreference electrode. Ferrocenium/ferrocene (Fc/Fc^+) redox potential was measured at the end of each experiment in order to calibrate the pseudoreference electrode as recommended by IUPAC.[33] Compounds **1−5** ($C = 1.0 \times 10^{-3}$ M in tetrahydrofuran) were drop-casted onto the GC-electrode and then dried. The GC-electrode was immersed into the electrochemical cell containing acetonitrile with 0.1 M tetrabutylammonium hexafluorophosphate ($TBAPF_6$). The compounds were electrochemically reduced prior to being oxidized between −3.0 V and +1.5 V at a scan rate of 20 mV/s.

2.3. Computational Methodology. Density functional theory (DFT) methods and especially the B3LYP one are extensively used in this kind of study. However, B3LYP and other hybrid functionals containing low percentage of Hartree−Fock exchange (%HF) are known to miss the dispersion interactions[34,35] which are important when considering the π-stacking interactions. This can affect for instance the dihedral angles between the conjugated rings of TPA−Th (TTh) molecules. In this case, the use of DFT methods containing higher %HF exchange may be necessary. In order to take into

account this effect, the M05-2X functional containing 56% of exact exchange was also considered.[36] The comparison between the B3LYP and M05-2X frontier orbital energies is shown in Figure S1 (Supporting Information). Due to the better agreement with the experimental results, only the B3LYP results will be discussed in the following.

The DFT calculations employing the B3LYP and M05-2X functionals were carried out by using the Gaussian 03 program.[37] The geometries of all the molecules were optimized by imposing a C_3 symmetry and by using the 6-31G* basis set. Frequency calculations were carried out to ensure that true minima were obtained. Tests for symmetry-relaxed geometry optimizations were also carried out, and negligible energy differences were observed. The geometry optimizations of the cationic radical species were carried out at the restricted open shell level.

The spectroscopic properties of the molecules were calculated by mean of time-dependent density functional theory method (TDDFT)[38−42] at the TDDFT/6-31+G*//DFT/6-31G* level. The HOMO and LUMO energies reported in this study were also obtained with the 6-31+G* basis set. The influence of greater basis sets (6-311++G**) on the HOMO and LUMO energies was also tested for the compounds **1** and **2**, and the results show only a small effect as compared to 6-31+G*.

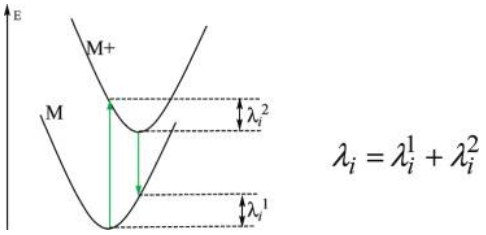

Figure 1. Schematic representation for the calculation of the internal reorganization energy, λ_i. The curves represent the potential energies of the neutral and the cationic species.

The calculation of the internal reorganization energies (λ_i) is shown schematically in Figure 1. Accordingly, the λ_i values are calculated as shown in the following equation[43]

$$\begin{aligned}\lambda_i &= \lambda_i^1 + \lambda_i^2 \\ &= \{E_M^{\text{GeometryM}^+} - E_M^{\text{GeometryM}}\} \\ &\quad + \{E_{M^+}^{\text{GeometryM}} - E_{M^+}^{\text{GeometryM}^+}\}\end{aligned} \tag{2}$$

where the quantity $E_M^{\text{GeometryM}^+}$ for instance corresponds to the energy of the neutral molecule M in the geometry of the cationic species M^+.

In view of the complexity of our molecules, the 6-31G* basis set was used for the calculation of the λ_i values which was shown to give negligible changes as compared to the 6-31G** basis set.[44]

3. RESULTS AND DISCUSSION

3.1. Geometries. The optimized geometries for all the molecules, along with some geometrical parameters, are presented in Figure 2. As generally observed for TPA derivatives, the three N−C bonds are coplanar, which is characteristic of enamines and indicates some degree of conjugation between the arms. Steric hindrance between the phenyl rings, grafted onto the central nitrogen atom, produces the typical propeller shape of the molecule. The dihedral angles between the adjacent conjugated rings in the compounds **1**−**5** (Figure 2) are in good agreement with previous calculations for these types of systems.[8,44]

The influence of the CH_3 group (mimicking the steric effect of the experimental nonyl group in our compounds) is reflected in the greater Ph−TTh dihedral angle obtained in the case of compound **1** as compared to compound **2** (42.8° and 27.6°, respectively). The same effect is observed when comparing compounds **4** and **5**. It can be expected that this difference should influence their packing properties during the formation of the solid films.

Finally, we note that all the dihedral angles in the cationic state are reduced by roughly 10°−15°, with the exception of the Ph−Ph dihedral angles which undergo a slight reduction of only ∼1−2° (Figure 2).

3.2. Electronic Structure and Electrochemical Properties. Cyclic voltammetry was performed to investigate the electrochemical properties and HOMO and LUMO energy levels of compounds **1**−**5**. These compounds were drop-casted onto the electrode from a THF solution resulting in a thin layer of **1**−**5** on the working electrode. As shown in Figure 3, all compounds exhibited n- and p-doping/dedoping (reduction/oxidation) processes. The n- doping was realized prior to the p-doping (as described in the Experimental section). In fact, p-doping was subsequently followed by a polymerization process (CV shown in Figure S2), since the α-carbon (in the vicinity of the sulfur atom) of the external thiophene ring is free. This was somewhat surprising because our calculations performed on the charged molecules (radical cations) reveal spin density mainly localized on the TPA core (58−34% for **1**−**5**, respectively, B3LYP/6-31G* level), whereas only 8% and 3% of the total spin density (compounds **1** and **5**, respectively) were found on each terminal heterocycle. In fact, during the p-doping, the reverse potential was chosen systematically far beyond the onset potential, hence bringing out the production of high concentration of radical cations in the layer and favoring the coupling of vicinal radical cation into a polymeric system. Hence the reverse scan of the p-doping process exhibits the reduction of the polymeric system. In the case of the n-doping, **4** and **5** exhibited a quasi-reversible reduction process while the three other compounds were irreversibly reduced. The origin of the reversibility of compounds **4** and **5** stands in their LUMO levels which are lower than those of compounds **1**−**3**, thus stabilizing the radical anion. Hence, the n-doping appears quasi-reversible.

The onset oxidation (or reduction) potential measures the potential at which the electron is withdrawn from the HOMO (or given to the LUMO). In the case of p-doping, the onset potentials, for **1**−**5**, range between 0.58 and 0.41 V vs Fc/Fc^+ (−2.68 and −2.35 V for the n-doping, Table 1). The HOMO and LUMO energy levels were calculated from the onset oxidation and reduction potentials.[45,46] The electrochemical data are summarized in Table 1.

As expected, adding TTh and Th conjugated groups to the TPA core in **1**−**5** makes the HOMO (LUMO) energies increase (decrease) resulting in decreasing HOMO−LUMO gaps. The same trends are obtained from the B3LYP calculations on the isolated molecules (Figure 4 and Table

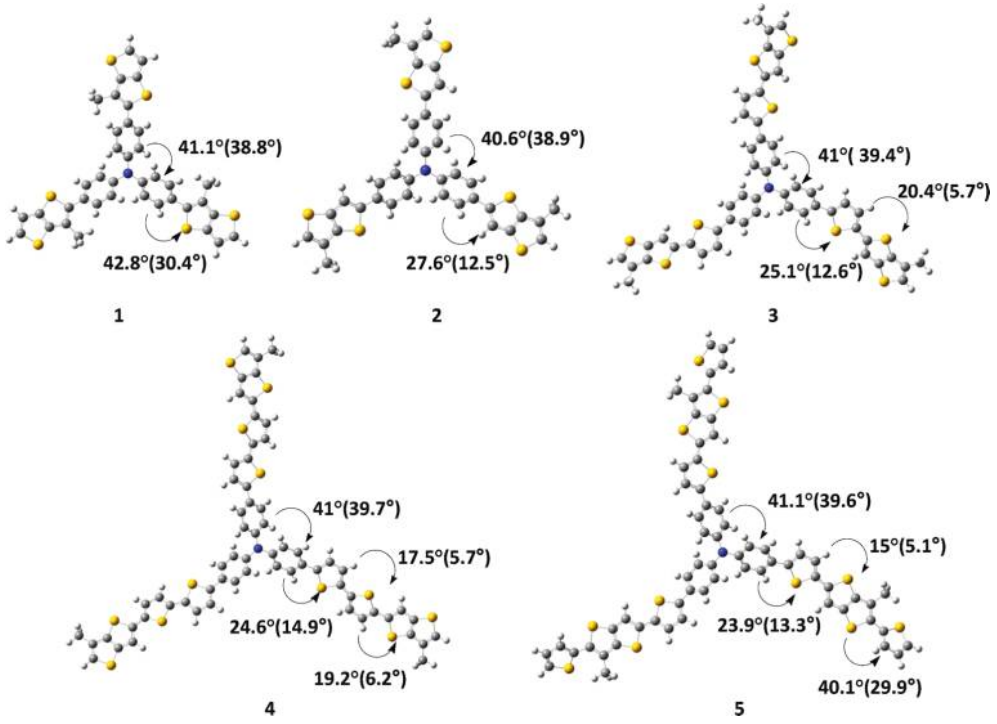

Figure 2. Optimized structures for the compounds **1**−**5**. Some typical dihedral angles (absolute values in degree) for the neutral and cationic (in parentheses) species are shown. Nitrogen, sulfur, carbon, and hydrogen atoms are shown respectively in blue, yellow, gray, and white colors.

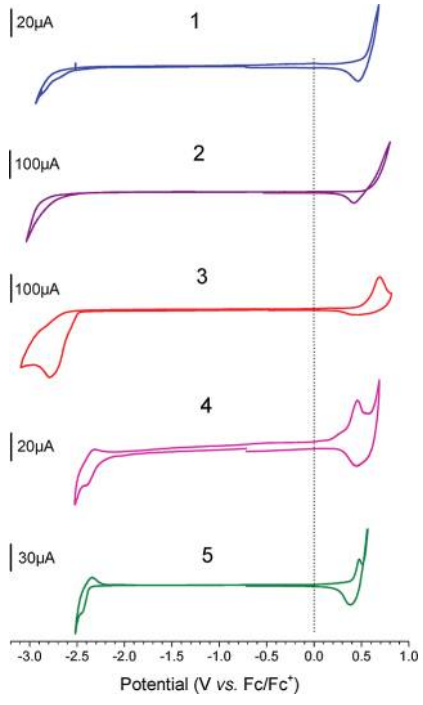

Figure 3. Cyclic voltammograms of thin films prepared by drop-casting from the compounds **1**−**5** on glassy carbon disk in 0.1 M $TBAPF_6$ in ACN.

1), indicating that the molecular packing forces do not significantly modify the intramolecular electronic structure. The differences between the theoretical and electrochemical values are a well-known consequence of performing calculations that lack medium-related factors. In spite of this, both approaches show similar trends in the evolution of the HOMO and LUMO levels.

Table 1. Onset Oxidation Potentials Obtained from the Electrochemical Measurements for Compounds 1−5 and the Corresponding HOMO and LUMO Energies and HOMO−LUMO Gaps (E_g^{ec})[a]

	E^{ox} onset (V)	E^{red} onset (V)	E_{HOMO} (eV)	E_{LUMO} (eV)	E_g^{ec} (eV)
1	0.58	−2.68	−5.38 (−5.15)	−2.12 (−1.54)	3.26 (3.60)
2	0.56	−2.46	−5.36 (−5.05)	−2.34 (−1.68)	3.02 (3.37)
3	0.54	−2.45	−5.34 (−4.98)	−2.35 (−2.02)	2.99 (2.96)
4	0.33	−2.27	−5.13 (−4.94)	−2.53 (−2.22)	2.60 (2.72)
5	0.41	−2.35	−5.21 (−4.96)	−2.45 (−2.16)	2.76 (2.80)

[a]In parentheses are presented the theoretical values calculated at the B3LYP/6-31+G* level.

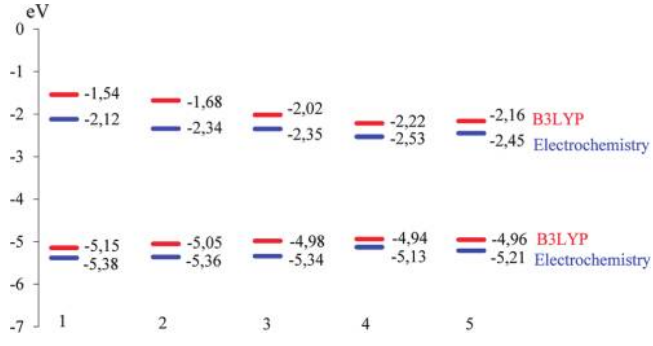

Figure 4. Comparison of the electrochemical and theoretical (B3LYP/6-31+G* level) HOMO and LUMO energies of compounds **1**−**5**.

In order to understand the difference in the way the HOMO and LUMO levels change, we focus on the nature of the frontier orbitals. The HOMO and LUMO pictograms for compounds **3**−**5** are presented in Figure 5 (Figure S3 for compounds **1** and **2**). The HOMO orbitals are mostly

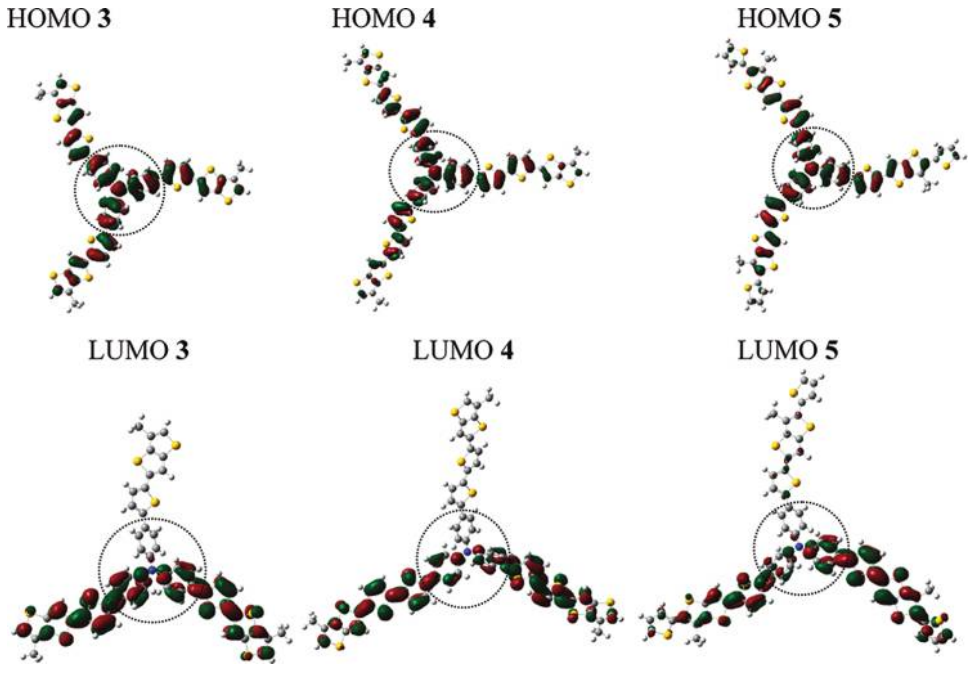

Figure 5. HOMO and LUMO pictograms for compounds **3**–**5** (B3LYP/6-31+G*). The encircled parts correspond to the TPA core.

developed in the TPA core with vanishing influence from the peripheral Th or TTh groups. This can be explained by considering, for instance, the HOMO of compound **2** as an antibonding combination of the local HOMO (TPA) core and the local HOMO (TTh): the HOMO (TPA) core is higher in energy than the TTh counterpart (−5.24 eV versus −6.09 eV, B3LYP/6-31+G* level) and will, therefore, provide a greater contribution to the total HOMO orbital. The energy difference between the local HOMO orbitals (the HOMO of a new Th or TTh group and the HOMO of TPA−TTh−$(Th)_n$) increases with the number of heterocycles in the arms, further reducing the contribution of the new heterocycles in the global HOMO orbital of the molecule. This effect should be reinforced by the presence of dihedral angles between the rings. The overall effect seems to be that, after three additional rings, the space extension of the total HOMO is almost negligible (Figure 5) indicating that the major influence of the peripheral heterocycles on the HOMO energy is predominantly inductive in nature.

Given that a good hole transfer implies a good overlap between the HOMO orbitals of two adjacent molecules, it is reasonable to suppose that increasing the number of conjugated heterocycles beyond a total of four in each arm should have little effect on the hole transfer.

As for the LUMO orbitals, there are, in each case, two quasi-degenerate virtual orbitals. In Figure 5, only the lower ones are presented for each compound. The extension of these orbitals mainly in the arms can be discussed in a similar way as for the HOMO orbitals. As a result, it is reasonable to expect that the influence of the last rings in the arms should be more significant for the LUMO energies, meaning that they are more influential on the spectroscopic properties and eventually on the electron mobility.

3.3. Optical Properties. The absorption spectra for the compounds **1**–**5** in films spin-coated from $CHCl_3$ solution ($C = 1.0 \times 10^{-5}$ M) are shown in Figure 6, while the optical characteristics are provided in Table 2.

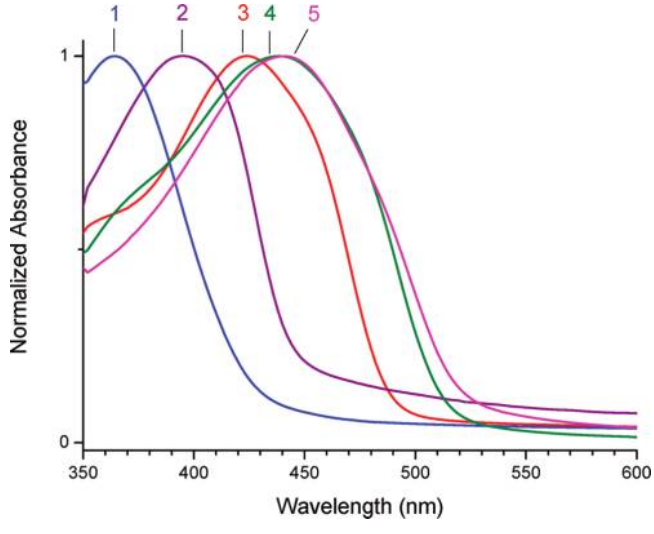

Figure 6. UV−vis absorption spectra for the compounds **1**–**5** (solid state) spin-coated from $CHCl_3$ solutions (1.0×10^{-5} M). The compound number is indicated on the top of each curve.

Broad absorption bands covering the wavelength range from 300 to 510 nm can be observed for all compounds in $CHCl_3$ solution, exhibiting λ_{max} which are red-shifted by roughly 74 nm when going from **1** to **5**. The absorption spectra measured in tetrahydrofuran (THF) exhibit the same trend as in chloroform and are presented in Table S1 (Supporting Information).

Compound **1** has the shortest λ_{max} value, probably due to the fact that it has the shortest conjugated chain length but also to the severe deplanarization caused by the steric hindrance induced by the nonyl chain. Displacing the nonyl chain to an external position in compound **2** induces a bathochromic effect of 32 nm due to a lower deviation in the molecular geometry from planarity. The λ_{max} values of **2**, **3**, and **4** show a progressive bathochromic shift when the length of the conjugated system is increased, exhibiting absorption maxima ranging from 386 nm for **2** to 422 nm for **4** in $CHCl_3$. This

Table 2. Energy of the $S_0 \rightarrow S_1$ Transitions from the TD-B3LYP/6-31+G* Calculations ($E_{S_0 \rightarrow S_1}$), Absolute (f) and Relative ($f/f(1)$) (with Respect to 1) Oscillator Strengths from the TD-B3LYP Calculations, Experimental λ_{max} Values, and Absolute (ε) and Relative ($\varepsilon/\varepsilon(1)$) (with Respect to 1) Extinction Molar Coefficients from the UV−Vis Spectra in Chloroform (1.0×10^{-5} M)

	TDB3LYP/6-31+G* (gas phase)			UV−vis			
	$E_{S_0 \rightarrow S_1}$ (eV)	f	$f/f(1)$	λ_{max} [$CHCl_3$][a] (nm)	λ_{max} [film][a](nm)	ε ($M^{-1}.cm^{-1}$)	$\varepsilon/\varepsilon(1)$
1	3.15	0.836	1.00	354 (3.50)	364 (3.41)	63000	1.00
2	2.96	0.903	1.08	386 (3.21)	396 (3.13)	77000	1.22
3	2.60	1.255	1.50	396 (3.13)	424 (2.92)	106000	1.68
4	2.39	1.725	2.06	422 (2.94)	444 (2.79)	128000	2.03
5	2.45	1.633	1.95	428 (2.90)	438 (2.83)	131000	2.08

[a]In parentheses are given the corresponding values in eV.

trend is in agreement with the trend previously reported in the case of homologous series of conjugated oligothiophene.[47,48] We finally note that the comparison of absorption signals between compounds **4** and **5** in $CHCl_3$, in which TTh−C_9 and Th units are combined in different orders, reveals only minor differences with a slightly longer λ_{max} for compound **5**.

Compared to their dilute solutions, the absorption bands in solid films are slightly red-shifted (10−28 nm). This red-shift can be related to the geometrical changes that occur in the solid films: the dihedral angles between adjacent rings in these molecules are reduced as is always observed when comparing gas-phase geometries to crystal structures[49] which, consequently, improves the π-conjugation and decreases the HOMO−LUMO gaps.

The theoretical UV−vis spectra for compounds **1**−**5** (Figure S4, Supporting Information) indicate that the λ_{max} values (410, 420, 478, 500, and 490 nm, respectively) are dominated by $S_0 \rightarrow S_1$ electronic transitions. The influence of higher excited states of the λ_{max} values is visible only for compounds **4** and **5** but does not modify the trend deduced from the $S_0 \rightarrow S_1$ transitions alone. The $S_0 \rightarrow S_1$ transition energies for compounds **1**−**5** are presented in Table 2 and show the same global trend as compared to the experimental λ_{max} values. Comparison between the relative experimental extinction molar coefficients and relative oscillator strengths (Table 2) also shows good overall agreement.

There is, however, a small ambiguity in the experimental results for compounds **4** and **5**. The experimental UV−vis spectra in solution suggest that the efficiency of the π-conjugation increases in the order of **1**−**2**−**3**−**4**−**5**, while the UV−vis spectra for solid films suggest a permutation in the order between **4** and **5**. The TD-DFT calculations and also the HOMO−LUMO gaps deduced from electrochemical measurements yield results which are in agreement with the UV−vis spectra in solid films.

These somewhat surprising results might be related to the conformational twists along the conjugated arms in solution where rotational barriers between the heterorings can be as low as ~10 kJ/mol.[50] The HOMO pictograms of compounds **4** and **5** (Figure 5) indicate that, in the case of **4**, there are more possible rotations between rings contributing significantly in the HOMO orbital. These conformational twists are not taken into account in the calculations and should also be less pronounced in solid state thus yielding the agreement between the respective results. Nevertheless, we note that the differences observed between the HOMO−LUMO gaps of compounds **4** and **5** are small (0.04 eV roughly) and may also be due to other factors.

3.4. Evaluation of Hole-Transfer Properties. In this paragraph we present a preliminary comparison of compounds **1**−**5** with respect to their intramolecular properties as hole-transporting materials. We remember that, in order to obtain high hole-transfer rate constants (k_{HT}), the electronic coupling parameter (t) should be maximized whereas the reorganization energy ($\lambda = \lambda_s + \lambda_i$) should be minimized (eq 1).

3.4.1. Internal Reorganization Energy (λ_i). The λ_i values for compounds **1**−**5** (calculated using eq 2) decrease from 0.219 eV (compound **1**) to 0.150 eV for the compound **4** (B3LYP/6-31G* level, Table S2). In terms of a monoelectronic description, this global trend suggests that the intramolecular geometry-relaxation energy should be smaller for systems with larger space delocalization in the HOMO orbital. While this observation might hold true for compounds with planar π-systems,[43,51] other factors could play in the opposite sense. Indeed, the λ_i values of compounds **1**−**5** are all higher than the value of 0.11−0.12 eV found for the TPA core (this work and ref 8, respectively). The reason may be related to the fact that adding Th or TTh groups increases the number of dihedral angles between adjacent rings which are very sensitive to changes in the number of electrons in the π-system. The decrease of the dihedral angles upon oxidation is coupled to changes in the bond lengths due to the increase in the π-conjugation efficiency, thus resulting in increased λ_i values (see also refs 8 and 44).

The importance of this effect can also be seen when comparing for instance the Ph−TTh dihedral angles of compounds **1** and **2** (42.8° and 27.6° respectively, neutral state) which could explain the corresponding λ_i values (0.219 and 0.188 eV, respectively). The same trend is observed when comparing the compounds **5** (λ_i = 0.173 eV) and **4** (λ_i = 0.150 eV) for which the TTh−Th dihedral angles are 40.1° and 19.2°, respectively. The smaller impact of this effect in the latter case could be explained by the smaller contribution of the peripheral rings on the HOMO orbital of **4** and **5** as compared to **1** and **2** (Figure 5).

Based on these λ_i values it can be deduced that the higher k_{HT} values should be observed for the compounds **3**, **4**, and **5.** Actually, the k_{HT} values estimated by considering a fixed value of the electronic coupling (t = 0.05 eV)[52] for all the compounds are multiplied by a factor of 3 when going from **1** to **5** (Table S2, Supporting Information calculations based on the Marcus−Levich−Jortner equation[53]). Admittedly, this change is small but shows the impact of λ_i on the relative hole-transfer rate constants of compounds **1**−**5**.

3.4.2. Electronic Coupling. Due to the size and shape of compounds **1**−**5,** the calculation of the electronic coupling

parameter (t) is not straightforward. However, the comparison of the space extension of their HOMO orbitals gives a good insight in this respect. Indeed, the HOMO orbitals of **1**−**5** are mostly developed in the TPA core while the influence of the Th or TTh groups vanishes with the distance from the center (Figure 5 and Figure S3). This implies that, in order for compounds **1**−**5** to exhibit good hole-transfer properties, a good overlap should be established between the central parts of the HOMO orbitals of two adjacent molecules. This observation suggest that the presence of the nonyl group in the proximity of the TPA core is expected to prevent significant overlap between the HOMO orbitals of adjacent molecules which, in turn, should have a negative influence on the transport properties. It can be then expected that compounds **3**, **4**, and **5**, in which the nonyl group is situated relatively far from the TPA core, exhibit efficient overlaps and non-negligible t values, which, according to the Marcus−Levich formula (eq 1), corresponds to faster hole transfer.

We finally note that both parameters discussed here (λ_i and t) work in "concert" and suggest that, from the molecular standpoint, the hole-transport properties of compounds **3**, **4**, and **5** should be better as compared to those of **1**−**2**.

4. CONCLUSIONS

Five star-shaped molecules with TPA core and various conjugated linkers such as thiophene and thieno[3,2-*b*]-thiophene−C_9H_{19} have been investigated using a combination of experimental and theoretical methods. Electrochemical measurements show the HOMO energy levels gradually increasing from −5.38 to −5.13 eV with the addition of Th or TTh groups while LUMO values decrease from −2.12 to −2.45 eV. Both interval values suggest for these compounds promising contact efficiency with common dyes or gold electrodes. In addition, the absorption bands for these materials are found to extend only slightly into the visible region.

The HOMO orbitals of compounds **4** and **5** are mostly localized in the central part of these molecules and exhibit negligible contribution from the peripheral Th or TTh groups, suggesting that adding another heterocyclic ring in compounds **4** or **5** would have minimal impact on their hole−mobility properties.

The above conclusions suggest that, in order to obtain good electron coupling between two adjacent molecules, a good overlap is necessary between the central parts of the frontier orbitals in these molecules. The presence of the nonyl group in the proximity of the TPA core is expected to negatively affect the transport properties.

Finally, the calculated reorganization energies (λ_i) are found to be relatively small and suggest better charge-transfer properties for compounds **3**, **4**, and **5**, which is in line with the conclusions drawn on the basis of the larger space extension of the HOMO orbitals and the positioning of the nonyl group in these molecules.

Based on this analysis it is concluded that the compounds **3**, **4**, and **5** possess interesting hole-transporting properties and can be good candidates for use in hybrid solar cells.

■ ASSOCIATED CONTENT

Supporting Information

HOMO and LUMO pictograms for compounds **1** and **2**; comparison between some dihedral angles obtained with B3LYP and M05-2X methods; comparison of frontier-orbital energies obtained with B3LYP and M05-2X methods with the values obtained from the electrochemical measurements; TDDFT UV−vis spectra for compounds **1**−**5**; absorption wavelengths measured in tetrahydrofuran (THF) solution; λ_i and k_{HT} values for the compounds **1**−**5.** This material is available free of charge via the Internet at http://pubs.acs.org.

■ AUTHOR INFORMATION

Corresponding Author

*E-mail: gjergji.sini@u-cergy.fr.

■ REFERENCES

(1) Oregan, B.; Gratzel, M. *Nature* **1991**, *353*, 737−740.
(2) Cai, N.; Moon, S. J.; Cevey-Ha, N.-L.; Moehl, T.; Humphry-Baker, R.; Wang, P.; Zakeeruddin, S. M.; Graetzel, M. *Nano Lett.* **2011**, *11*, 1452−1456.
(3) Bach, U.; Lupo, D.; Comte, P.; Moser, J. E.; Weissortel, F.; Salbeck, J.; Spreitzer, H.; Gratzel, M. *Nature* **1998**, *395*, 583−585.
(4) Snaith, H. J.; Moule, A. J.; Klein, C.; Meerholz, K.; Friend, R. H.; Gratzel, M. *Nano Lett.* **2007**, *7*, 3372−3376.
(5) Strohriegl, P.; Grazulevicius, J. V. *Adv. Mater.* **2002**, *14*, 1439−1452.
(6) Shirota, Y. *J. Mater. Chem.* **2000**, *10*, 1−25.
(7) Shirota, Y. *J. Mater. Chem.* **2005**, *15*, 75−93.
(8) Malagoli, M.; Bredas, J. L. *Chem. Phys. Lett.* **2000**, *327*, 13−17.
(9) He, C.; He, Q. G.; Yi, Y. P.; Wu, G. L.; Bai, F. L.; Shuai, Z. G.; Li, Y. F. *J. Mater. Chem.* **2008**, *18*, 4085−4090.
(10) He, C.; He, Q. G.; Yang, X. D.; Wu, G. L.; Yang, C. H.; Bai, F. L.; Shuai, Z. G.; Wang, L. X.; Li, Y. F. *J. Phys. Chem. C* **2007**, *111*, 8661−8666.
(11) He, C.; He, Q. G.; Wu, G. L.; Bai, F. L.; Li, Y. F. *Proc. SPIE—Int. Soc. Opt. Eng.* **2007**, *6656*, 66560.
(12) Wu, G. L.; Zhao, G. J.; He, C.; Zhang, J.; He, Q. G.; Chen, X. M.; Li, Y. F. *Sol. Energy Mater. Sol. Cells* **2009**, *93*, 108−113.
(13) He, C.; He, Q. G.; He, Y. J.; Li, Y. F.; Bai, F. L.; Yang, C. H.; Ding, Y. Q.; Wang, L. X.; Ye, J. P. *Sol. Energy Mater. Sol. Cells* **2006**, *90*, 1815−1827.
(14) Unger, E. L.; Ripaud, E.; Leriche, P.; Cravino, A.; Roncali, J.; Johansson, E. M. J.; Hagfeldt, A.; Boschloo, G. *J. Phys. Chem. C* **2010**, *114*, 11659−11664.
(15) Hagberg, D. P.; Marinado, T.; Karlsson, K. M.; Nonomura, K.; Qin, P.; Boschloo, G.; Brinck, T.; Hagfeldt, A.; Sun, L. *J. Org. Chem.* **2007**, *72*, 9550−9556.
(16) Hagberg, D. P.; Yum, J. H.; Lee, H.; De Angelis, F.; Marinado, T.; Karlsson, K. M.; Humphry-Baker, R.; Sun, L. C.; Hagfeldt, A.; Gratzel, M.; Nazeeruddin, M. K. *J. Am. Chem. Soc.* **2008**, *130*, 6259−6266.
(17) Metri, N.; Sallenave, X.; Beouch, L.; Plesse, C.; Goubard, F.; Chevrot, C. *Tetrahedron Lett.* **2010**, *51*, 6673−6676.
(18) Bassler, H. *Phys. Status Solidi B* **1993**, *175*, 15−56.
(19) Coropceanu, V.; Cornil, J.; da Silva, D. A.; Olivier, Y.; Silbey, R.; Bredas, J. L. *Chem. Rev.* **2007**, *107*, 926−952.
(20) Olivier, Y.; Lemaur, V.; Bredas, J. L.; Cornil, J. *J. Phys. Chem. A* **2006**, *110*, 6356−6364.
(21) Marcus, R. A. *Rev. Mod. Phys.* **1993**, *65*, 599−610.
(22) Levich, V. G. *Adv. Electrochem. Electrochem. Eng.* **1966**, *4*, 249−371.
(23) Marcus, R. A. *J. Chem. Phys.* **1956**, *24*, 966−978.
(24) Marcus, R. A.; Sutin, N. *Biochim. Biophys. Acta* **1985**, *821*, 265−322.
(25) Sakanoue, K.; Motoda, M.; Sugimoto, M.; Sakaki, S. *J. Phys. Chem. A* **1999**, *103*, 5551−5556.
(26) Leriche, P.; Frere, P.; Cravino, A.; Aleveque, O.; Roncali, J. *J. Org. Chem.* **2007**, *72*, 8332−8336.
(27) Zhao, G. J.; Wu, G. L.; He, C.; Bai, F. Q.; Xi, H. X.; Zhang, H. X.; Li, Y. F. *J. Phys. Chem. C* **2009**, *113*, 2636−2642.
(28) Li, R. Z.; Lv, X. J.; Shi, D.; Zhou, D. F.; Cheng, Y. M.; Zhang, G. L.; Wang, P. *J. Phys. Chem. C* **2009**, *113*, 7469−7479.

(29) Xu, M. F.; Wenger, S.; Bala, H.; Shi, D.; Li, R. Z.; Zhou, Y. Z.; Zakeeruddin, S. M.; Gratzel, M.; Wang, P. *J. Phys. Chem. C* **2009**, *113*, 2966−2973.
(30) Kohn, W.; Sham, L. J. *Phys. Rev.* **1965**, *140*, A1133−A1138.
(31) Lee, C. T.; Yang, W. T.; Parr, R. G. *Phys. Rev. B* **1988**, *37*, 785−789.
(32) Becke, A. D. *J. Chem. Phys.* **1993**, *98*, 5648−5652.
(33) Gritzner, G.; Kuta, J. *Pure Appl. Chem.* **1984**, *56*, 441−466.
(34) Allen, M. J.; Tozer, D. J. *J. Chem. Phys.* **2002**, *117*, 11113−11120.
(35) Tsuzuki, S.; Luthi, H. P. *J. Chem. Phys.* **2001**, *114*, 3949−3957.
(36) Zhao, Y.; Schultz, N. E.; Truhlar, D. G. *J. Chem. Theory Comput.* **2006**, *2*, 364−382.
(37) Frisch, M. J.; Trucks, G. W.; Schlegel, H. B.; Scuseria, G. E.; Robb, M. A.; Cheeseman, J. R.; Montgomery, J. A., Jr.; Vreven, T.; Kudin, K. N.;et al. *Gaussian 03*, revision. E01; Gaussian, Inc.: Pittsburgh, PA.
(38) Gross, E. K. U.; Kohn, W. *Phys. Rev. Lett.* **1985**, *55*, 2850−2852.
(39) Runge, E.; Gross, E. K. U. *Phys. Rev. Lett.* **1984**, *52*, 997−1000.
(40) Gross, E. K. U.; Kohn, W. *Adv. Quantum Chem.* **1990**, *21*, 255−291.
(41) Bauernschmitt, R.; Ahlrichs, R. *Chem. Phys. Lett.* **1996**, *256*, 454−464.
(42) Casida, M. E.; Jamorski, C.; Casida, K. C.; Salahub, D. R. *J. Chem. Phys.* **1998**, *108*, 4439−4449.
(43) Bredas, J. L.; Beljonne, D.; Coropceanu, V.; Cornil, J. *Chem. Rev.* **2004**, *104*, 4971−5003.
(44) Lin, B. C.; Cheng, C. P.; Lao, Z. P. M *J. Phys. Chem. A* **2003**, *107*, 5241−5251.
(45) Liu, B.; Yu, W. L.; Lai, Y. H.; Huang, W. *Chem. Mater.* **2001**, *13*, 1984−1991.
(46) Wagner, P.; Aubert, P. H.; Lutsen, L.; Vanderzande, D. *Electrochem. Commun.* **2002**, *4*, 912−916.
(47) Kirschbaum, T.; Azumi, R.; Mena-Osteritz, E.; Bauerle, P. *New J. Chem.* **1999**, *23*, 241−250.
(48) Thomas, K. R. J.; Hsu, Y. C.; Lin, J. T.; Lee, K. M.; Ho, K. C.; Lai, C. H.; Cheng, Y. M.; Chou, P. T. *Chem. Mater.* **2008**, *20*, 1830−1840.
(49) Cailleu, H.; Baudour, J. L.; Zeyen, C. M. E. *Acta Crystallogr., Sect. B* **1979**, *35*, 426−432.
(50) Brédas, J.-L.; Heeger, A. *Macromolecules* **1990**, *23*, 1150−1156.
(51) Deng, W.-Q.; Goddard, W. A. III. *J. Phys.Chem. B* **2004**, *108*, 8614−8621.
(52) The fixed electronic coupling for all the compounds (t = 0.05 eV) is not an assumption, but only a way to separate the effect of this parameter on k_{HT} from the effect of the reorganization energy parameter.
(53) Jortner, J. *J. Chem. Phys.* **1976**, *64*, 4860−4867.